The Effect of a Random Crystal-Field on the Mixed Ising Spins $\left(\frac{1}{2}, \frac{3}{2}\right)$

L. Bahmad, M.R. Benayad, A. Benyoussef and A. El Kenz*

Faculté des Sciences, Département de Physique, Laboratoire de Magnétisme et Physique des Hautes Energies, B.P. 1014, Rabat, Morocco

(Received October 22, 2010; in final form January 4, 2011)

We study the magnetic properties of a mixed Ising ferrimagnetic system, in which the two interacting sublattices have spins σ, $(\pm\frac{1}{2})$ and spins S, $(\pm\frac{3}{2}, \pm\frac{1}{2})$ in the presence of a random crystal field, with the mean field approach. The results obtained, using mean field approach and Monte Carlo simulation, show the appearance of a new ferrimagnetic phase, namely the partly ferrimagnetic phase $(m_\sigma = \frac{-1}{2}, m_S = +1)$. Consequently, three topologically different types of phase diagrams have been given by mean field approach. The effect of increasing the exchange interaction parameter J, at very low temperature is also investigated.

PACS: 05.50.+q, 75.10.Hk, 75.50.Gg

1. Introduction

Recently, many authors have studied both experimentally and theoretically the magnetic properties of mixed spins 1/2 and spins $S > 1/2$ Ising system, with a crystal field interaction. In fact, crystal-field interaction effects on the transition temperature have been investigated by several methods such as effective field theory [1–4], finite cluster approximation [5], mean field theory [6], Migdal–Kadanof renormalisation group method [7] and cluster variational method [8]. Nevertheless, some disagreements between theoretical studies, such as the existence of tricritical points, have occurred. Experimental studies have shown that the complex MnNi(EDTA)–$6H_2O$ is a good example of a mixed spin system [9].

On the other hand, important advances have been made in the synthesis of two- and three-dimensional ferrimagnets, such as $2d$ organo-metallic ferrimagnets [10, 11], and $2d$ networks of the mixed-metal materials $[P(Phenyl)_4][MnCr(oxalate)_3]_n$ [12]. Other interests in the mixed spin Ising models can be related to the modelling of magnetic structures suitable for describing a ferrimagnetism of certain classes of insulating materials. In fact, the mixed systems provide simple but interesting models to study molecular magnetic materials and magneto-optical recording materials [13, 14]. Furthermore, the appearance of many compensation points in a variety of ferrimagnetic systems has been pointed out theoretically [15, 16]. Since the ferrimagnetic order plays an important role in these materials, the investigation of ferrimagnetism in mixed spin systems has rapidly become a field of interest. As these systems consist of two interpenetrating and nonéquivalent sublattices, they have lower translational symmetry than their single-spin counterparts.

On the other hand, many different methods have been employed in the study of the mixed spin 1/2 and spin 1 Ising model [17, 18], and this system has been solved exactly in special cases. Nevertheless, new magnetic properties and compensation behaviors are found for mixed spins in the presence of a crystal-field [19] as they were predicted by Néel theory of ferrimagnetism [20].

The mean-field theory approach, based on the bogolyubov inequality for the gibbs free energy [21], showed that the obtained phase diagrams exhibit a variety of multicritical points such as tricritical points and isolated critical points. on the other hand, we have shown in some of our recent works [22, 23] the existence of interesting properties in the magnetization behavior and phase diagrams in the presence of a random crystal-field.

The purpose of this work is to study, using the mean field approximation (MFA), the influence of crystal-field disorder on the phase diagrams and magnetization of a mixed-spin ferrimagnetic Ising system, in which the two interpenetrating sublattices have spin values $\sigma = \pm\frac{1}{2}$ and $S = \pm\frac{3}{2}, \pm\frac{1}{2}$. The most interesting result emerging from this study is the appearance of different types of phase diagrams, in the particular case of two-valued distribution of crystal-field. Consequently, three topologically different types of phase diagrams occur. This paper is organized as follows: in Sect. 2, we introduce the model and give the details of the MFA. The ground-state phase

* corresponding author; e-mail: elkenz@fsr.ac.ma

diagram is discussed in Sect. 3. In Sect. 4 we present and discuss our results. Finally, in Sect. 5 we give our conclusions.

2. Model and method

The MFA method is used to study the behavior of complex spin systems, such as the ferrimagnetic mixed Ising models. The model we are studying consists of two interpenetrating sublattices. One sublattice has spins σ assumed to take the values $\pm\frac{1}{2}$, the other sublattice has spins S that can take four values: $\pm\frac{3}{2}$, and $\pm\frac{1}{2}$. The spins S have only the spins σ as nearest neighbors and vice versa. The interaction between the spins σ and S is assumed to be an antiferromagnetic exchange. The Hamiltonian of this model is written as

$$\mathcal{H} = J\sum_{\langle ij\rangle}\sigma_i S_j + \sum_{i=1}^{N/2}\Delta_i S_i^2\,, \tag{1}$$

where N is the total number of lattice sites. The exchange interaction parameter J is assumed to be positive. The first summation is carried out only over nearest pairs of spins and Δ_i is a quenched random crystal field distributed according to the probability distribution [22–25]:

$$\mathcal{P}(\Delta_i) = \frac{1}{2}\left[\delta(\Delta_i - \Delta(1+\alpha)) + \delta(\Delta_i - \Delta(1-\alpha))\right]\,, \tag{2}$$

where α is a positive constant.

An analogous probability distribution has been used to investigate the critical behavior of ^{3}He–^{4}He mixtures in random media (aerogel) modeled by the spin 1 Blume–Capel model. In this model, a negative crystal-field value represents the field at the pore-grain interface and a positive value is a bulk field that controls the concentration of ^{3}He atoms [26–28].

The variational principle based on the Gibbs–Bogolyubov inequality for the free energy per site is described by [29–31]:

$$\mathcal{F} \leq \Phi = -T\log(Z_0) + \langle\mathcal{H} - \mathcal{H}_0\rangle_0\,. \tag{3}$$

One can denote by h_σ and h_S the molecular fields associated with the order parameters $m_\sigma = \langle\sigma\rangle_0$ and $m_S = \langle S\rangle_0$, respectively, expressed as

$$h_\sigma = J\sum_{j=1}^{z}\langle S_j\rangle_0 = zJm_S\,, \tag{4}$$

$$h_S = J\sum_{j=1}^{z}\langle\sigma_j\rangle_0 = zJm_\sigma\,, \tag{5}$$

where z is the number of nearest neighbors and $\langle\ldots\rangle_0 = \frac{\mathrm{Tr}\ldots\exp(-\beta\mathcal{H}_0)}{\mathrm{Tr}\exp(-\beta\mathcal{H}_0)}$, denotes the average value performed over the Hamiltonian $\mathcal{H}_0$.

The effective Hamiltonian of the system is given by

$$\mathcal{H}_0 = h_\sigma\sum_{i=1}^{N/2}\sigma_i + h_S\sum_{i=1}^{N/2}S_i + \sum_{i=1}^{N/2}\Delta_i S_i^2\,. \tag{6}$$

The partition function generated by the above Hamiltonian is given by

$$\begin{aligned} Z_0 = \mathrm{Tr}\left(\exp\left(-\frac{\mathcal{H}_0}{T}\right)\right) &= \left[2\cosh\left(\frac{\beta h_\sigma}{2}\right)\right]^{N/2} \\ &\times\left[2\exp\left(\frac{-9\beta\Delta_i}{4}\right)\cosh\left(\frac{3\beta h_S}{2}\right)\right. \\ &\left.+\,2\exp\left(\frac{-\beta\Delta_i}{4}\right)\cosh\left(\frac{\beta h_S}{2}\right)\right]^{N/2}, \end{aligned} \tag{7}$$

where T is absolute temperature and $\beta = 1/T$. Boltzmann's constant has been set to unity. The total free energy is given by

$$\begin{aligned} \Phi &= \frac{NJzm_\sigma m_S}{2} - \frac{Nh_\sigma m_\sigma}{2} - \frac{Nh_S m_S}{2} \\ &- NT\int\log(Z_0)\mathcal{P}(\Delta_i)\,\mathrm{d}\Delta_i\,. \end{aligned} \tag{8}$$

After the integration over the probability distribution, the free energy per spin is expressed as

$$\begin{aligned} \frac{\Phi}{N} &= \frac{Jzm_\sigma m_S}{2} - \frac{h_\sigma m_\sigma}{2} - \frac{h_S m_S}{2} \\ &- \frac{T}{2}\left[\log\left(2\cosh\frac{h_\sigma}{2T}\right)\right. \\ &+\frac{1}{2}\left(\log\left(2\exp\left(-\frac{9\Delta(1+\alpha)}{4T}\right)\cosh\left(\frac{3h_S}{2T}\right)\right.\right. \\ &\left.+\,2\exp\left(-\frac{\Delta(1+\alpha)}{4T}\right)\cosh\left(\frac{h_S}{2T}\right)\right) \\ &+\log\left(2\exp\left(-\frac{9\Delta(1-\alpha)}{4T}\right)\cosh\left(\frac{3h_S}{2T}\right)\right. \\ &\left.\left.\left.+\,2\exp\left(-\frac{\Delta(1-\alpha)}{4T}\right)\cosh\left(\frac{h_S}{2T}\right)\right)\right)\right]. \end{aligned} \tag{9}$$

In order to investigate the magnetization of the system, the order parameters m_σ and m_S are defined by minimizing the free energy.

The mean-field equations of state are given by

$$m_\sigma = -\frac{1}{2}\tanh\left(\frac{z}{2t}Jm_S\right)\,, \tag{10}$$

and

$$m_S = -\frac{1}{2}\left(\frac{A}{B} + \frac{C}{D}\right)\,, \tag{11}$$

where

$$A = 3\exp\left(-\frac{9d}{4t}(1+\alpha)\right)\sinh\left(\frac{3zm_\sigma}{2t}\right)$$

$$+\exp\left(-\frac{d}{4t}(1+\alpha)\right)\sinh\left(\frac{zm_\sigma}{2t}\right),$$

$$B = 2\exp\left(-\frac{9d}{4t}(1+\alpha)\right)\cosh\left(\frac{3zm_\sigma}{2t}\right)$$

$$+2\exp\left(-\frac{d}{4t}(1+\alpha)\right)\cosh\left(\frac{zm_\sigma}{2t}\right),$$

$$C = 3\exp\left(-\frac{9d}{4t}(1-\alpha)\right)\sinh\left(\frac{3zm_\sigma}{2t}\right)$$

$$+\exp\left(-\frac{d}{4t}(1-\alpha)\right)\sinh\left(\frac{zm_\sigma}{2t}\right),$$

$$D = 2\exp\left(-\frac{9d}{4t}(1-\alpha)\right)\cosh\left(\frac{3zm_\sigma}{2t}\right)$$

$$+2\exp\left(-\frac{d}{4t}(1-\alpha)\right)\cosh\left(\frac{zm_\sigma}{2t}\right).$$

In the above equations, and in all that follow, t and d denote the reduced temperature T/J and the reduced crystal field Δ/J, respectively. The coordination number z is set to 4 (square lattice).

The solutions of Eqs. (10)–(11) are not unique, the stable solutions are those minimizing the free energy Eq. (9), while the solutions are unstable. If the order parameters are continuous (discontinuous), the transitions are of second (first) order.

3. Ground state

The ground state phase diagram of the system under investigation is illustrated in Fig. 1. Indeed, for very low temperatures and depending on the values of $\alpha \geq 0$ and the reduced crystal field d. Equations (10)–(11) lead to three solutions: $(m_\sigma = \frac{-1}{2}, m_S = \frac{3}{2})$, $(m_\sigma = \frac{-1}{2}, m_S = \frac{1}{2})$, and $(m_\sigma = \frac{-1}{2}, m_S = 1)$. By comparing the energies of all configurations, we established the ground state phase diagram. This phase diagram is drawn in the reduced (d, α) plane. One can distinguish four cases:

1) For $\alpha = 0$, a first order transition point between the phase $(m_\sigma = -\frac{1}{2}, m_S = \frac{3}{2})$ and the phase $(m_\sigma = \frac{-1}{2}, m_S = \frac{1}{2})$ occurs at $d = +1$.

2) For $0 < \alpha < 1$, two first-order transition lines occur: one between the phase $(m_\sigma = -\frac{1}{2}, m_S = \frac{3}{2})$ and the phase $(m_\sigma = \frac{-1}{2}, m_S = 1)$ separated by the equation line $d = z/[4(1+\alpha)]$ and the other between the phase $(m_\sigma = \frac{-1}{2}, m_S = 1)$ and the phase $(m_\sigma = \frac{-1}{2}, m_S = \frac{1}{2})$ separated by the equation line $d = z/[4(1-\alpha)]$.

3) For $\alpha = 1$, a first order transition point between the phase $(m_\sigma = \frac{-1}{2}, m_S = \frac{3}{2})$ and the ferrimagnetic phase $(m_\sigma = \frac{-1}{2}, m_S = 1)$ appears at $d = \frac{1}{2}$.

4) For $\alpha > 1$, two first-order transition lines between the $(m_\sigma = \frac{-1}{2}, m_S = 1)$ phase and the $(m_\sigma = \frac{-1}{2}, m_S = \frac{3}{2})$ phase and the $(m_\sigma = \frac{-1}{2}, m_S = \frac{3}{2})$ phase and the $(m_\sigma = \frac{-1}{2}, m_S = 1)$ phase occur at $d = z/[4(1-\alpha)]$ and $d = z/[4(1+\alpha)]$, respectively.

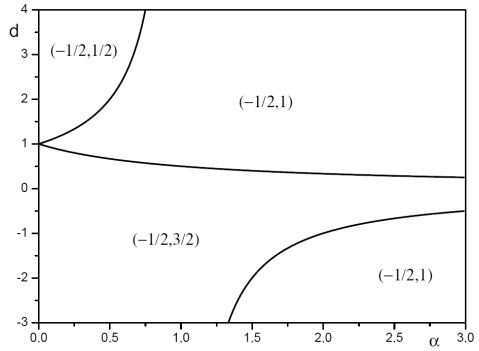

Fig. 1. The ground state phase diagram established in the (d, α) plane. $(m_\sigma = \frac{-1}{2}, m_S = \frac{1}{2})$, $(m_\sigma = \frac{-1}{2}, m_S = \frac{3}{2})$ and $(m_\sigma = \frac{-1}{2}, m_S = 1)$ are the only stable phases at very low temperature.

It is worth to note that for $d = 0$, only the phase $(m_\sigma = \frac{-1}{2}, m_S = \frac{3}{2})$ is stable at $T = 0$ K, and $\alpha = 0$ corresponds to mixed spin $(m_\sigma = \frac{1}{2}, m_S = \frac{3}{2})$ model with nonrandom crystal-field.

4. Phase diagrams and discussions

4.1. Phase diagrams

A detailed discussion dealing with finite temperature phase diagrams is presented in this section. For this purpose, we solve numerically Eqs. (9), (10) and (11). A rich variety of phase diagrams is observed both when varying α in the $(t_c = T_c/J, d)$ plane, and d in the (t_c, α) plane. The critical temperature is plotted as a function of d for $\alpha = 0$ (Fig. 2a), $\alpha = 0.5$ (Fig. 2b), $\alpha = 1$ (Fig. 2c) and $\alpha = 2$ (Fig. 2d). In Fig. 2a, the paramagnetic $(m_\sigma = 0, m_S = 0)$ and ferrimagnetic phases $(m_\sigma = \frac{-1}{2}, m_S = \frac{3}{2})$ and $(m_\sigma = \frac{-1}{2}, m_S = \frac{1}{2})$ are separated by a second-order transition line. A first--order transition line separating the above phases is observed at very low temperature. This first-order transition line is terminated by an isolated critical point located at $(d_{tr} = 1, t_{tr} = 0.06)$. Above this last point, a continuous passage occurs between the two ferrimagnetic phases. Whereas, for $\alpha = 0.5$ (Fig. 2b), two first--order transition lines appear at low temperature. The first one separates the phases $(m_\sigma = \frac{-1}{2}, m_S = \frac{3}{2})$ and $(m_\sigma = \frac{-1}{2}, m_S = 1)$, and terminates at an isolated critical point located at $d_{tr} = 0.667, t_{tr} = 0.11$. The second first-order transition line separates the ferrimagnetic phases $(m_\sigma = \frac{-1}{2}, m_S = 1)$ and $(m_\sigma = \frac{-1}{2}, m_S = \frac{1}{2})$, and terminates at an isolated critical point located at $d_{tr} = 2, t_{tr} = 0.04$.

In Fig. 2c, plotted for $\alpha = 1$, the phase $(m_\sigma = \frac{-1}{2}, m_S = \frac{1}{2})$ is absent at low temperature and the only first--order transition line, present in this region, separates

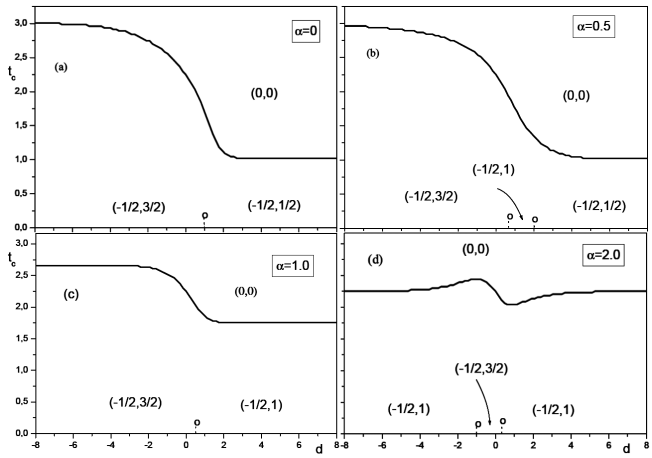

Fig. 2. The critical temperature as a function of d plotted for: $\alpha = 0$ (a), $\alpha = 0.5$ (b), $\alpha = 1$ (c) and $\alpha = 2$ (d). The full lines correspond to the second-order transitions, whereas the dashed lines represent the first-order transitions. The tiny circles denote isolated critical points.

the phases $(m_\sigma = \frac{-1}{2}, m_S = \frac{3}{2})$ and $(m_\sigma = \frac{-1}{2}, m_S = 1)$, and terminated at an isolated critical point located at $(d_{\rm tr} = 0.5, t_{\rm tr} = 0.09)$.

In Fig. 2d, the system exhibits two first-order transition lines, at very low temperature, terminated by two isolated critical points: the first at $d = -1, t = 0.11$ and the second located at $d = \frac{1}{3}, t = 0.19$. The two lines separate the phases $(m_\sigma = \frac{-1}{2}, m_S = 1)$ and $(m_\sigma = \frac{-1}{2}, m_S = \frac{3}{2})$, and the phases $(m_\sigma = \frac{-1}{2}, m_S = \frac{3}{2})$ and $(m_\sigma = \frac{-1}{2}, m_S = 1)$, respectively.

It is worthwhile to note that our results concerning the appearance, at low temperature, of first-order transition line terminated by an isolated critical point is in agreement with other works as MFA [6] and Monte Carlo [32, 33]. To give more details concerning the first-order transition lines, the free energy and entropy of the system are calculated at low temperature. The free energy and entropy are plotted as function of d for $t = 0.035$ and two α values: 0.25 and 1, in Fig. 3a and b, respectively. In agreement with Fig. 2b and c, a discontinuous change of the free energy slope at first-order transition temperatures is observed. Consequently the entropy is discontinuous at these temperatures (see inset of Fig. 3a and b). For the second-order transition lines, the total free energy and entropy are plotted versus temperature, for $\alpha = 0.25$ and $d = -3$ (see Fig. 3c). The entropy varies discontinuously at a second-order transition temperature. As consequence, the specific heat will exhibit a discontinuity at this transition temperature.

In order to outline the effect of the parameter α we plot, in Fig. 4, the transition temperatures $t_{\rm c}$ for several values of the crystal field d. Indeed, for $d = 2$, Fig. 4a shows the existence of a second-order transition line between the paramagnetic and the ferrimagnetic phases and a first-order transition between the ferrimagnetic phases

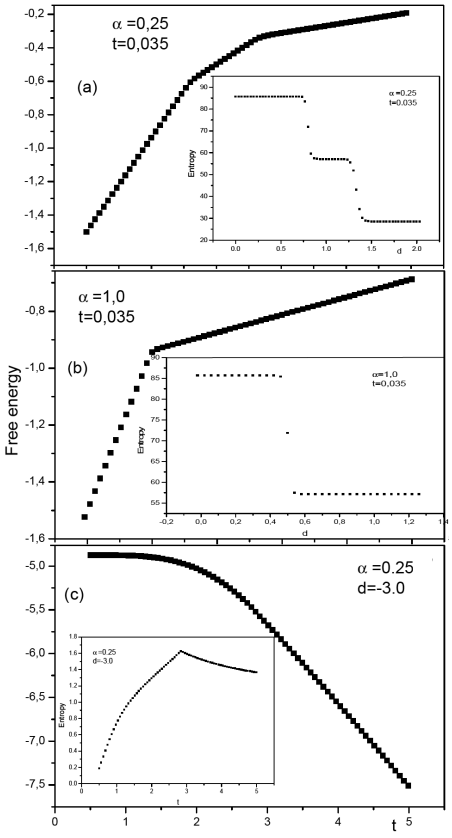

Fig. 3. In (a) and (b), the free energy and entropy (from expressions developed at low temperature) are plotted versus the reduced crystal-field d for $t = 0.035$ and two α values: 0.25 and 1, respectively. In (c), the same physical quantities are plotted as a function of temperature for $\alpha = 0.25$ and $d = -3$.

$(m_\sigma = \frac{-1}{2}, m_S = \frac{1}{2})$ and $(m_\sigma = \frac{-1}{2}, m_S = 1)$ terminated at an isolated critical point, $\alpha = 1.5, t = 0.055$. Whereas for $d = 0$ (Fig. 4b), the second order transition line from the ferrimagnetic phase to the paramagnetic phase is independent of α because of the absence of the crystal-field. A first order transition line separating the phases $(m_\sigma = \frac{-1}{2}, m_S = \frac{3}{2})$ and $(m_\sigma = \frac{-1}{2}, m_S = 1)$ is obtained for $d = -1$ as shown in Fig. 4c, which terminates at an isolated critical point $\alpha = 2, t = 0.09$ between the ferrimagnetic and partly ferrimagnetic phases. At high temperatures, a second-order transition line between the ferrimagnetic phase and the paramagnetic phase is found. To complete this study, the effect of increasing the exchange interaction parameter J, at very low temperature, keeping α constant have been investigated. The results we found for low temperature and selected values of α, showed that the transitions obtained in the ground state phase diagram (Fig. 1) are still present. For $\alpha = 0.5$, Fig. 5a shows that the system can exhibit the phases $(m_\sigma = \frac{-1}{2}, m_S = \frac{3}{2})$, $(m_\sigma = \frac{-1}{2}, m_S = 1)$ and $(m_\sigma = \frac{-1}{2}, m_S = \frac{1}{2})$ when increasing the parameter Δ at any constant coupling J value. For $\alpha = 1$, the system un-

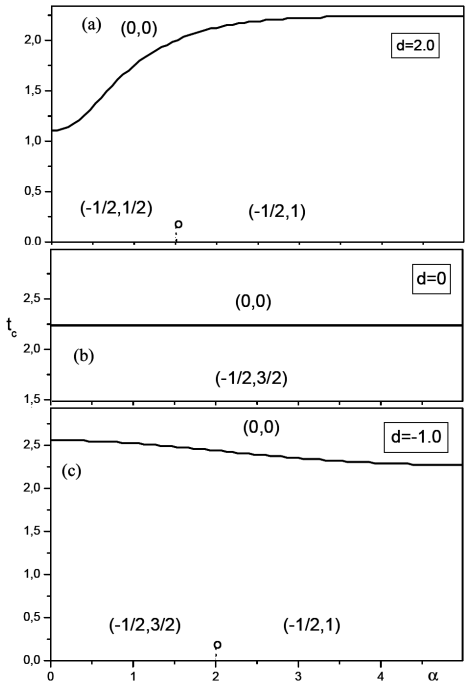

Fig. 4. The transition temperatures t_c as a function of the parameter α for selected values of the crystal field: $d = 2$ (a), $d = 0$ (b), and $d = -1$ (c).

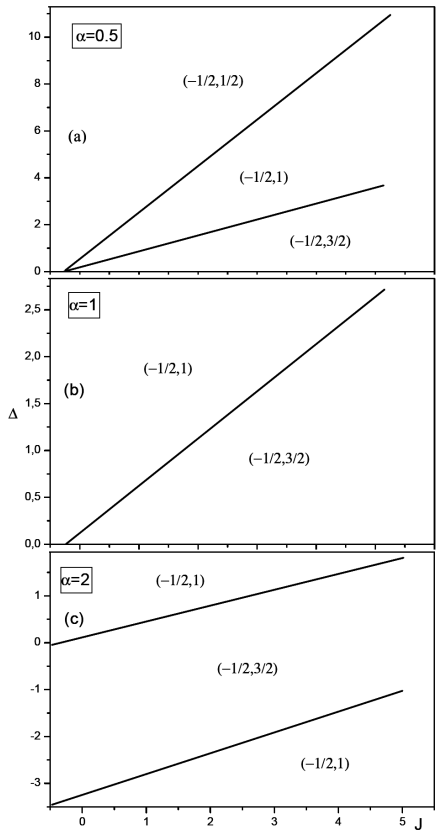

Fig. 5. Phase diagrams in the plane (Δ, J), at very low temperature $t = 0.025$ for $\alpha = 0.5$ (a), $\alpha = 1$ (b) and $\alpha = 2$ (c). In (a) the system exhibits the phases $(m_\sigma = \frac{-1}{2}, m_S = \frac{1}{2})$, $(m_\sigma = \frac{-1}{2}, m_S = 1)$ and $(m_\sigma = \frac{-1}{2}, m_S = \frac{3}{2})$, in (b) the system undergoes a transition from the phase $(m_\sigma = \frac{-1}{2}, m_S = 1)$ to the phase $(m_\sigma = \frac{-1}{2}, m_S = \frac{3}{2})$, while (c) shows the phases $(m_\sigma = \frac{-1}{2}, m_S = \frac{1}{2})$, $(m_\sigma = \frac{-1}{2}, m_S = 1)$ and $(m_\sigma = \frac{-1}{2}, m_S = \frac{3}{2})$ when increasing the exchange interaction parameter J for fixed values of the crystal field Δ.

dergoes a transition from the phase $(m_\sigma = \frac{-1}{2}, m_S = \frac{3}{2})$ to the phase $(m_\sigma = \frac{-1}{2}, m_S = 1)$ when increasing the crystal field Δ (see Fig. 5b). For a large value of α ($\alpha = 2$), Fig. 5c shows that the effect of increasing the parameter Δ on the phase transitions is to favour the phase $(m_\sigma = \frac{-1}{2}, m_S = 1)$.

4.2. Magnetic properties

In this section, we focus our interest on the magnetizations which charaterise the various phases seen in the previous phase diagrams as a function of the crystal field d and the parameter α, for fixed temperature values. Figure 6a–c shows the temperature dependence of magnetizations as a function of d for $\alpha = 0$, $\alpha = 0.5$ and $\alpha = 1$, respectively. In Fig. 6a, the magnetization m_S shows a jump and a continuous passage from $\frac{3}{2}$ to $\frac{1}{2}$ at temperatures below and above the temperature corresponding to the isolated critical point, respectively. Figure 6b shows a double jump in the magnetization m_S, at a very low temperature, from $\frac{3}{2}$ to 1 and from 1 to $\frac{1}{2}$, and a continuous passage at a temperature greater than the temperature corresponding to the isolated critical points. The same behaviour of the magnetization m_S, found in Figs. 6a and b is also seen in Fig. 6c for $\alpha = 1$. This is in agreement with Fig. 2c.

The re-entrant behavior found in Fig. 2d, is well illustrated in Figs. 7a and b, where the magnetizations m_σ and m_S are plotted, for $\alpha = 2$, at two temperatures $t = 2.2$ and $t = 2.3$, respectively. Figure 7a shows that for $t = 2.2$, the magnetizations m_σ, m_S and consequently $M = (m_\sigma + m_S)/2$ drop to zero in the region $0 < d < 3.5$. This is in good agreement with Fig. 2d. On the other hand, Fig. 7b shows that for a higher temperature ($t = 2.3$) this phenomenon is inverted in the region $-3 < d < 0$, so that the magnetizations m_σ, m_S, and consequently $M = (m_\sigma + m_S)/2$, are zero outside of this region. This is once again in agreement with Fig. 2d.

The behavior of the magnetizations m_σ, m_S, and $M = (m_\sigma + m_S)/2$ as a function of the parameter α for fixed values of crystal field and temperature has been investigated. Figure 8a and b shows these magnetizations as a function of α for $d = 2, t = 2$ and $d = -1, t = 2.5$, respectively. Figure 8a shows that for positive values of the crystal field, the effect of the increasing α values is to favorize the ordered phase, in a region of temperatures lower than t_c. For a negative value of the crystal field,

this phenomenon is inverted as it is shown in Fig. 8b, plotted for $d = -1$. One can note that the results found in Fig. 8a and b, are in good agreement with those illustrated in Fig. 4a and c, respectively. On the other hand, it is obvious that the magnetizations are independent of the parameter α in the absence of a crystal field, as is well illustrated in Fig. 4b.

In order to confirm the appearance of the partly ferrimagnetic phase ($m_\sigma = \frac{-1}{2}, m_S = 1$) found from the MFA calculations, Monte Carlo simulations implemented under the Metropolis algorithm have been performed. Indeed, a square lattice of linear size $L = 180$ with periodic boundary conditions have been considered. The initial 20000 MCS (Monte Carlo steps) until the system enters in a stationary regime are discarded. Then, more than 10000 MCS have been used to calculate the averages of the quantities of interest, namely the sublattice magnetizations per spin, $\langle m_\sigma \rangle = \frac{1}{N}\sum_i \sigma_i$ and $\langle m_{\boldsymbol{S}} \rangle = \frac{1}{N}\sum_i \boldsymbol{S}_i$.

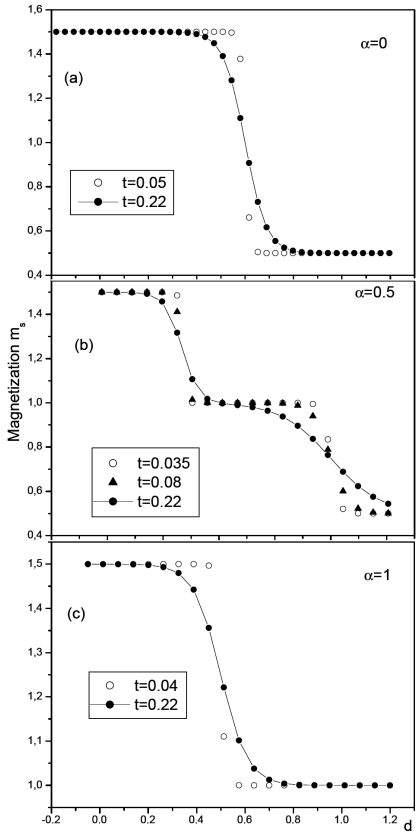

Fig. 6. The magnetization m_S as a function of the reduced crystal-field d for a fixed value of α at fixed reduced temperatures value: $\alpha = 0$ and ($t = 0.05$ and $t = 0.22$) (a), $\alpha = 0.5$ and ($t = 0.0035$, $t = 0.08$ and $t = 0.22$) (b) and $\alpha = 1$ ($t = 0.04$ and $t = 0.22$) (c), respectively.

Figure 9 shows the sublattice magnetisations for $\alpha = 0.5$ and $d = 0.5$ (a), $d = 1$ (b) and $d = 3$ (c). It is clearly seen from Fig. 9a–c that the sublattice magnetizations m_S starts at $T = 0$ K at $m_S = 3/2$, 1 and $1/2$, respec-

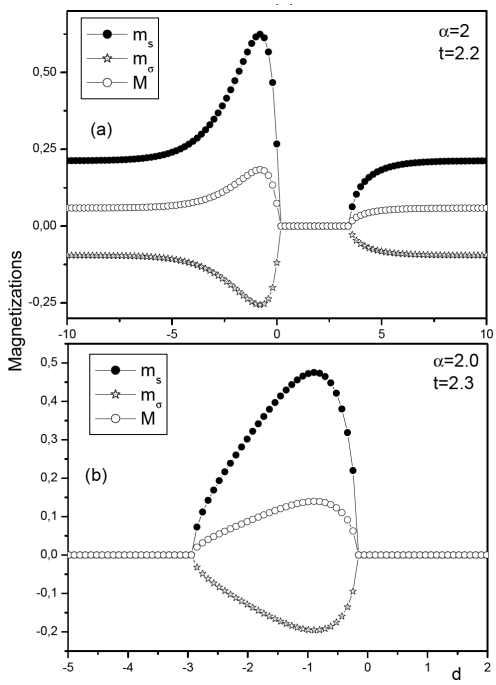

Fig. 7. The magnetizations m_S, m_σ and $M = (m_\sigma + m_S)/2$ as functions of the reduced crystal-field d for $\alpha = 2$, and two temperature values: $t = 2.2$ (a) and $t = 2.3$ (b), respectively.

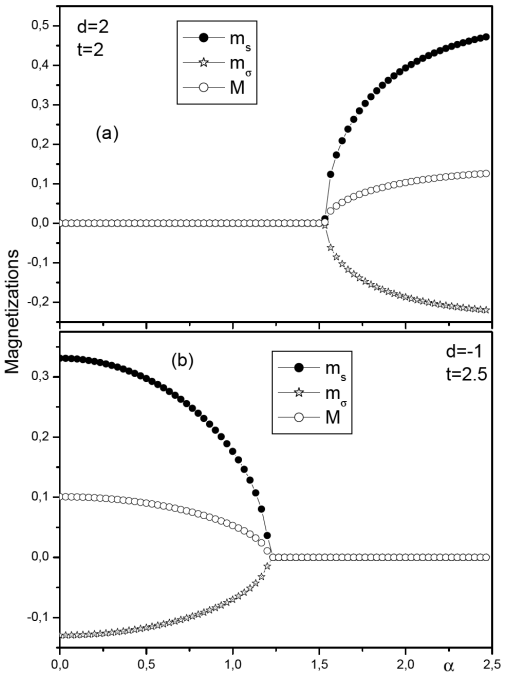

Fig. 8. The magnetizations m_σ, m_S, and $M = (m_\sigma + m_S)/2$ as function of the parameter α for fixed crystal field values and temperature ($d = 2, t = 2$) in (a) and ($d = -1, t = 2.5$) in (b).

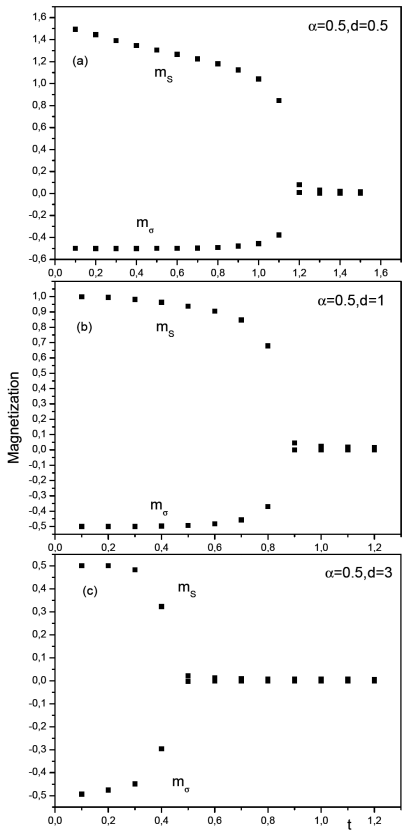

Fig. 9. The magnetizations m_σ and m_S as function of the reduced temperature t for a fixed value of $\alpha = 0.5$ and selected reduced crystal-field: $(d = 0.5)$ (a), $(d = 1)$ (b), and $(d = 3)$ (c).

tively. This is in accordance with the ground-state phase diagram (Fig. 1) and with the results given by MFA calculation.

5. Conclusions

We have investigated the effect of random crystal-field on the magnetic properties of a mixed spin $\sigma = \frac{1}{2}$ and spin $S = \frac{3}{2}$ Ising model on a square lattice, using the mean field approximation (MFA). Our results revealed many interesting phenomena, namely, several topologically different types of phase diagrams. This is due to the appearance of a new ferrimagnetic phase, namely $(m_\sigma = \frac{-1}{2}, m_S = 1)$, in the studied system. Furthermore, these phase diagrams present rich varieties of phase transitions with first and second order phase transition lines. The first-order transition lines terminate at isolated critical points. On the other hand, the compensation phenomenon appears in the system. This is due to the fact that the ferrimagnetic mixed spin $(\sigma = \frac{1}{2}, S = +1)$ exhibits a compensation phenomenon as given in other works. Also the effect of increasing the exchange interaction parameter J, at very low temperature, when keeping α constant, is investigated. The magnetization behaviors as a function of the parameters α and d, are also studied.

References

[1] T. Kaneyoshi, *Physica A* **153**, 556 (1988).

[2] T. Kaneyoshi, *J. Magn. Magn. Mater.* **92**, 59 (1990).

[3] A. Benyoussef, A. El Kenz, T. Kaneyoshi, *J. Magn. Magn. Mater.* **131**, 173 (1994).

[4] A. Benyoussef, A. El Kenz, T. Kaneyoshi, *J. Magn. Magn. Mater.* **131**, 179 (1994).

[5] N. Benayad, A. Klumper, J. Zittartz, A. Benyoussef, *Z. Phys. B* **77**, 333 (1989).

[6] O.F. Abubrig, D. Horvath, A. Bobak, M. Jascur, *Physica A* **296**, 437 (2001).

[7] N. Benayad, J. Zittartz, *Z. Phys. B* **81**, 107 (1990).

[8] J.W. Tucker, *J. Magn. Magn. Mater.* **237**, 437 (2001).

[9] M. Drillon, E. Coronado, D. Beltran, R. Georges, *J. Chem. Phys.* **79**, 449 (1983).

[10] H. Tamaki, Z.J. Zhong, N. Matsumoto, S. Kida, M. Korkawa, N. Archiwa, Y. Yashimoto, H. Okawa, *J. Ann. Chem. Soc.* **114**, 6974 (1992).

[11] H. Okawa, N. Matsumoto, H. Tamaki, S. Kida, M. Ohba, *Mol. Cryst. Liq. Cryst.* **233**, 257 (1993).

[12] C. Mathoniere, C.J. Nuttall, S.G. Carlin, P. Day, *Inorg. Chem.* **351**, 201 (1996).

[13] E. Albayrak, *Physica A* **375**, 174 (2007).

[14] J. Li, G. Wei, A. Du, *Physica B* **368**, 121 (2005).

[15] T. Kaneyoshi, *Phys. Rev. B* **52**, 7304 (1995).

[16] M. Jascur, *Physica A* **252**, 217 (1998).

[17] A. Dakhama, *Physica A* **252**, 225 (1998).

[18] J. Octmaa, W. Zheng, *Physica A* **328**, 185 (2003).

[19] S. Yana, L. Liua, *J. Magn. Magn. Mater.* **312**, 285 (2007).

[20] A. Bobak, M. Jascur, *Phys. Rev. B* **51**, 11533 (1995).

[21] A. Bobak, F.O. Abubrig, *Phys. Rev. B* **68**, 224405 (2003).

[22] L. Bahmad, A. Benyoussef, A. El Kenz, *Phys. Rev. B* **76**, 094412 (2007).

[23] L. Bahmad, A. Benyoussef, A. El Kenz, *Physica A* **387**, 825 (2008).

[24] N. Boccara, A. El Kenz, M. Saber, *J. Phys. Condens. Matter* **1**, 5721 (1989).

[25] A.P. Vieira, J.X. de Carvalho, S.R. Salinas, *Phys. Rev. B* **63**, 184415 (2001).

[26] A. Maritan, M. Cieplak, M.R. Swift, F. Toigo, J.R. Banavar, *Phys. Rev. Lett.* **69**, 221 (1992).

[27] C. Buzano, A. Maritan, A. Pelizzola, *J. Phys. Condens. Matter* **6**, 327 (1994).

[28] N.S. Branco, B.M. Boechat, *Phys. Rev. B* **56**, 11673 (1997).

[29] N.N. Bogoliubov, *J. Phys. (USSR)* **11**, 23 (1947).

[30] R.P. Feynmann, *Phys. Rev.* **97**, 660 (1955).

[31] J.J. Binney, N.J. Dowrick, A.J. Fisher, M.E.J. Newman, *The Theory of Critical Phenomena*, Clarendon Press, Oxford 1992.

[32] D. Peno Lara, J.A. Plascak, *Physica A* **260**, 443 (1998).

[33] G. Wei, Q. Zhang, Y. Gu, *J. Magn. Magn. Mater.* **301**, 245 (2006).